RMetS
Royal Meteorological Society

Characteristics of cold pools observed in narrow valleys and dependence on external conditions

P. F. Sheridan,* S. B. Vosper and A. R. Brown
Met Office, Exeter, UK

*Correspondence to: P. F. Sheridan, Met Office, FitzRoy Road, Exeter EX1 3PB, UK.
E-mail: peter.sheridan@metoffice.gov.uk

Observations from the recent COLd-air Pooling EXperiment (COLPEX) field campaign are used to relate the intensity of cold pools within two small valleys (O(100 m) depth and O(1 km) width) to flow conditions within the airmass passing over the valley. The temperature structure of the cold pools is examined using transects of ground-based sensors through the valleys and radiosonde releases from within the valley, in order to evaluate simple two-dimensional concepts of cold-pool formation due to sheltering. The cold-pool spatial and temporal structure is found to be consistent between different nights when strong cold pools occurred. Initially a sharp surface inversion occurs similarly at all points within the valley, with isentropes roughly terrain-parallel. The inversion layer at the bottom of the valley then grows deeper, spreading over the bottom portion of the valley, and cross-valley isentropes eventually become horizontal. By defining appropriate measures of the relative temperature drop within the cold pool, and non-dimensional valley depth diagnosed with respect to the speed and stability of the approaching flow, the measurements are shown to be consistent with previous relationships determined for simple two-dimensional valleys.

Key Words: stable boundary layer; complex terrain; hill; drainage; sheltering; temperature; COLPEX

Received 21 August 2012; Revised 19 February 2013; Accepted 18 March 2013; Published online in Wiley Online Library 22 May 2013

Citation: Sheridan PF, Vosper SB, Brown AR. 2014. Characteristics of cold pools observed in narrow valleys and dependence on external conditions. *Q. J. R. Meteorol. Soc.* **140**: 715–728. DOI:10.1002/qj.2159

1. Introduction

High spatial variability of near-surface temperatures in complex terrain represents a significant forecasting challenge. Rapid horizontal fluctuations may occur within short distances, particularly on calm, clear nights, typically when radiative cooling of the surface leads to rapid cooling of the adjacent air, resulting in a strong temperature inversion. In sheltered areas protected from winds which would normally break up sharp temperature gradients, localised cold pools form, where crop damage and hazards such as fog and road icing are more likely than over flat open ground in the same region. Frequently the scale of cold pools is beneath the grid scale of operational numerical weather prediction (NWP) models and temperatures must be predicted by post-processing the NWP output in order to account for local terrain effects (e.g. Sheridan *et al.*, 2010). An understanding of terrain-related processes such as sheltering and drainage which govern the cold pool structure, intensity (temperature drop within the cold pool) and lapse rate on these scales is required in order to develop and improve post-processing methods.

In major mountain ranges, for instance in broad alpine valleys, the formation of cold pools is complicated by the presence of vigorous, coherent thermal katabatic flows. These are generated by the cooling of air over slopes, which results in substantial hydrostatic pressure differences over the scale of the terrain (Whiteman, 1990; Zängl, 2004). Drainage currents transport colder air towards and down the valley bottom, assisting cold pool growth but, due

to their strength, are also likely to increase turbulent mixing with warmer air aloft, potentially weakening vertical temperature gradients. While sheltering from the synoptic flow assists cold pool formation in such terrain, again interactions through channelling effects, such as pressure-driven channelling, have been found to impact the evolution of the nocturnal valley atmosphere (Zängl, 2009). It is not clear in general to what extent drainage and channelling significantly affect the structure and properties of cold pools in gentler terrain. Recent studies suggest that in smaller valleys the sheltering provided by surrounding terrain may be the primary cause of cold air pooling (e.g. Gustavsson *et al.*, 1998; Clements *et al.*, 2003; Vosper and Brown, 2008; Bodine *et al.*, 2009). The mechanism for this is the reduction of turbulent mixing within the valley as it becomes more difficult for the external flow over the hill tops to influence the valley bottom. Normally, over flat ground, as the surface cools radiatively, near-surface air also cools due to downward sensible heat flux at the surface and radiative flux divergence, but this is countered to an extent by downward turbulent mixing of warmer air from aloft. In the sheltered valley bottom the latter factor is reduced, but cooling factors are more or less as before. Thus a cold pool forms *in situ*. The process is enhanced the more effectively sheltered the valley bottom. The distribution of cold air within the valley by thermally driven flow is then a secondary factor. When sheltering is so effective that the valley bottom is essentially isolated from the external flow, the valley bottom is said to be 'decoupled'. In the Meteor Crater experiment (METCRAX), Arizona, this picture was further complicated by the intrusion of a cold, highly stable regional katabatic drainage flow which was able to enter the basin atmosphere (Savage *et al.*, 2008; Yao and Zhong, 2009; Whiteman *et al.*, 2010; Haiden *et al.*, 2011; Kiefer and Zhong, 2011), impacting temperatures near the surface and aloft. Vosper and Brown (2008) used two-dimensional (2D) idealised simulations to study the formation of cold pools for a range of overnight radiative cooling strengths and wind speeds. They found that the flow across the valley top developed a gravity wave structure. The degree of penetration of the external flow into the valley atmosphere, and hence the extent of the sheltered 'pocket' in which a cold pool could easily form, was controlled by the value of the non-dimensional valley depth, $\widetilde{N}H/\widetilde{U}$ (where $\widetilde{N}$ is the Brunt–Väisälä frequency, H the valley depth and $\widetilde{U}$ the wind speed in a layer near the surface). One of the main findings of Vosper and Brown (2008) was that deepening a valley enhanced the degree of cooling of the valley bottom, but beyond a critical non-dimensional valley depth no further enhancement occurred. Results consistent with this were also found in high-resolution simulations of real valleys (Smith *et al.*, 2010). The relationship of sheltering to the non-dimensional valley depth and its critical value was discovered in an earlier study using a towing tank by Bell and Thompson (1980) (though they refer to the inverse phenomenon of valley venting and the reciprocal of non-dimensional valley depth). While the synoptic-scale patterns under which cold pool formation is favoured are well-studied (e.g. Iijima and Shinoda, 2000; Daly *et al.*, 2009; Reeves and Stensrud, 2009), and numerous other studies have highlighted the correlation of near-surface wind speed with temperatures in valley bottoms, the Vosper and Brown result characterises the direct impact of the external flow and its structure on the valley atmosphere and cold pool formation from a dynamical point of view. In real valleys, three-dimensional (3D) processes such as down-valley drainage may affect cold pool structure, but sheltering is still likely to be a first-order effect in cold pool formation, and so the non-dimensional valley depth should retain importance. Gravity waves were also found to be significant when explaining warm-air intrusions into Arizona's Meteor Crater during METCRAX. Adler *et al.* (2012) used a conceptual model involving a gravity wave akin to a hydraulic jump at the crater's windward lip. However, unlike the simulations of Vosper and Brown (2008), this was shaped by the characteristic structure of the impinging mesoscale drainage flow, and the unusual shape of the crater's terrain.

A field campaign, the COLd-air Pooling EXperiment (COLPEX; Price *et al.*, 2011), was carried out in Shropshire, UK, in order to make a detailed study of the behaviour of nocturnal temperatures in small-scale complex terrain. A main aim of the project is the improvement of techniques for post-processing NWP data to account for local terrain in weather forecasts and assessment of high-resolution model performance. Note that Vosper *et al.* (2013) used the Met Office Unified Model (MetUM) at high resolution to gain insight into a case-study from COLPEX. The array of ground-based instruments used during COLPEX, supplemented during Intensive Observation Periods (IOPs) by radiosonde releases, allow a detailed analysis of cold pools and how their formation is influenced by the external flow conditions. The terrain is similar in scale to the crater studied during METCRAX (Whiteman *et al.*, 2008), and the idealised valleys studied by Vosper and Brown (2008), but is part of a complex valley system, in a moist climate, and without the presence of a tilted plain such as that which causes regional drainage flows to accompany cold pool formation at the Meteor Crater. Various sinkholes on a similar scale have also been studied in the US, the Alps and Japan (Iijima and Shinoda, 2000; Clements *et al.*, 2003; Whiteman *et al.*, 2004b; Steinacker *et al.*, 2007), although in these studies large orography is present sufficiently nearby to significantly impact the flow experienced over and within the basin, and the sinkhole areas are more wooded. Also, the already low temperatures experienced at such elevations can further enhance cooling in valley bottoms due to air-drying effects which impact the radiation budget (Whiteman *et al.*, 2007), and the presence of snow for a large part of the year, which strongly affects the heat flux budget (Whiteman *et al.*, 2004b; Zängl, 2005).

This article examines cold pool structure and nocturnal evolution during COLPEX, and adapts the concept used by Vosper and Brown (2008) to demonstrate how cold pool formation in real, O(1 km) wide valleys is linked to the vertical structure of the flow approaching the valley. For this reason the Vosper and Brown study is summarised in more detail in section 2. The COLPEX measurements are described in section 3. Cold pool structure and evolution are examined in section 4. In section 5 case-studies are used to demonstrate dependence of cold pools on external flow conditions. In section 6 quantitative relationships to the external vertical structure are established and conclusions are summarised in section 7.

2. Summary of Vosper and Brown (2008)

Vosper and Brown (2008) used idealised 2D simulations to study the formation of cold pools when varying the depth of an isolated valley within a plain, performing simulations with a range of background wind profiles (uniform wind with height), and F_{lw} values, where F_{lw} is the ratio of downwelling to upwelling long-wave radiative flux. F_{lw} represents the fraction of upwelling long-wave radiation which fails to escape the atmosphere; the closer its value is to 1, the weaker radiative cooling of the surface. The conditions resulted in a wide range of cold pool intensities. Cold pool intensity is defined as the largest negative overnight value of $\theta_{\mathrm{min}} - \overline{\theta}$, where θ_{min} is the minimum within the valley of the potential temperature at the lowest model level, and $\overline{\theta}$ the domain average of the potential temperature at the lowest model level. For a given valley depth, the intensity of the cold pool was controlled uniquely by the values of U and F_{lw}. Cold pool intensity increased with valley depth, H (the difference in height between the valley bottom and external plain), as the valley bottom became more sheltered from advection and turbulent mixing, but beyond a critical depth no further intensification occurred for a given wind profile and F_{lw}. When cold pool intensity was plotted against the non-dimensional valley depth, $\widetilde{N}H/\widetilde{U}$, the results showed that a critical value of $\widetilde{N}H/\widetilde{U}$ existed, beyond which cold pool intensification stalled, in the range 0.35–0.64. $\widetilde{N}$ and $\widetilde{U}$ represent overnight averages over the whole domain of, respectively, Brunt–Väisälä frequency calculated as a bulk value using differences in potential temperature between a level at H above ground and the lowest model level, and a simple average of the wind over the same layer. The temperature and wind profiles used for this were taken from 1D simulations carried out in order to generate initial profiles for the 2D simulations. Bell and Thompson (1980), using an obstacle containing a series of consecutive valleys with a roughly v-shaped cross-section, quote a threshold value of Froude number for valley venting of 1.3, or a non-dimensional valley depth equal to the reciprocal of this, 0.76.

3. Description of measurements

The COLPEX field campaign was conducted for 15 months during 2009–2010, focussing on detailed measurement of the boundary layer in and near the Clun valley, Shropshire, UK (52.43°N, 3.14°W), relief roughly 150 m, in order to observe the process of cold pool formation in stable nocturnal conditions. A variety of instruments were deployed, including mast-mounted sensors, radiosondes, an instrumented car, Doppler LIDAR and microwave radiometer, and are described in detail by Price *et al.* (2011). Measurements from ground-based temperature sensors and radiosonde releases are used here. Ground-based instrument sites are shown in Figure 1. The sites comprise a 50 m and two 30 m masts, instrumented for measurement of wind, temperature, moisture, pressure, visibility, and turbulent, ground and radiative flux components, ten Automatic Weather Stations (AWS), instrumented for wind, temperature, humidity and pressure, and 22 HOBO sensors, predominantly measuring only screen temperature. Data from screen- and mast-top-level temperature sensors are used in this study. The sites are arranged mostly in cross- and along-valley transects in the Clun and Burfield valleys

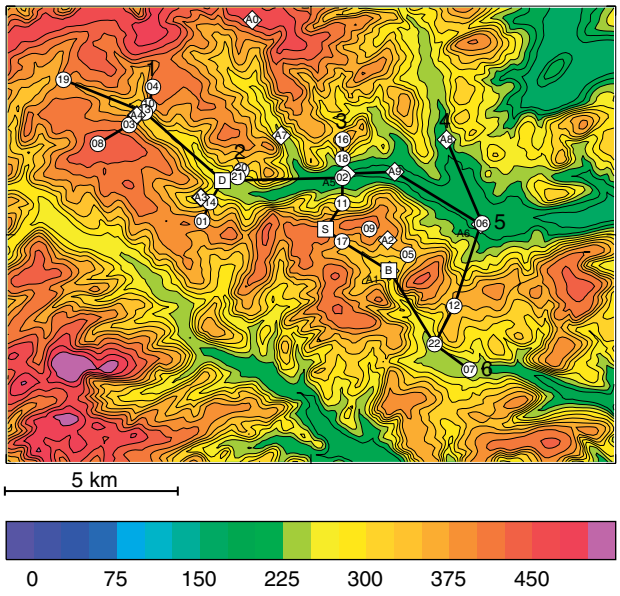

Figure 1. Locations of ground-based COLPEX sites in the Clun and Burfield valleys. Masts are shown as squares labelled 'D' (Duffryn), 'B' (Burfield), and 'S' (Springhill), AWSs as numbered diamonds and HOBO sites as numbered circles. Where HOBOs and AWSs are collocated, the AWS number is shown to the left of the site. Cross- and along-valley transects within the array have been indicated and numbered for reference within the text. Terrain heights are shaded, with contour interval 25 m.

(the transects have been numbered 1 to 6 in Figure 1). The roughly linear Clun valley is the larger of the two, containing more instrumentation (including the principal site, Duffryn, marked 'D') than the smaller Burfield valley (the mast on the main Burfield site is marked 'B'), which is more bowl-shaped at its head with a narrower neck leading through to a lower region. The third mast is located at Springhill on top of an intervening hill (marked 'S'). Measurements of the full radiative budget at screen level at the mast sites allowed the degree of radiative cooling to be summarised using F_{lw}.

Radiosondes were released from Duffryn at hourly intervals into the night during IOPs, with typically a small number of releases the next morning shortly before or after sunrise, with roughly concurrent releases from either Springhill or Burfield. The measurements have been supplemented by Met Office NWP forecast data at 4 km resolution (produced using the UK4 configuration of MetUM; Davies *et al.*, 2005; Lean *et al.*, 2008) to supply a continuous dataset of hourly vertical profiles of wind and temperature during IOP and non-IOP nights. These were used to calculate background values of Brunt–Väisälä frequency, N, and wind, U over the lowest 150 m above ground (roughly equal to the depth of the Duffryn site below the highest mast site at Springhill), analogous to $\widetilde{N}$ and $\widetilde{U}$ used by Vosper and Brown (2008) to study how cold pool formation responds to background wind strength and stability. In this capacity the UK4 data have an advantage in the fact that the valleys under study are not resolved, and the UK4 orography in the area is rather bland, so the profiles are not terrain-disturbed (as is the case for the 1D simulation profiles used for this purpose by Vosper and Brown, 2008). This is crucial since, for instance, using vertical profiles from within a valley to estimate the stability and speed of the approach flow and relating this to decoupling in the valley would lead to self-consistent results since typically decoupled valley atmospheres are stable and motion is weak.

N was calculated as a bulk value over the 150 m layer using differences in potential temperature between a level at 150 m and the lowest model level, and U as a simple average over the same layer, for the grid point closest to the Duffryn site. A similar method was the basis of NH/U values used by Smith *et al.* (2010) in an analysis of cold pool intensity within high-resolution model simulations of real valleys.

4. Examination of cold-pool structure

A comprehensive climatology of cold pools is beyond the scope of this article (though Price *et al.*, 2011, summarise the frequency of cold pools of different strengths). However, an examination of cold pool structure and repeatability using representative cases selected from the strongest cold pooling nights is useful in order to establish a consistent method for quantifying cold pool intensity more generally, and to ensure that the measure of intensity used fairly represents a generic quality of the cold pool which can be compared meaningfully between cases. This section describes case-studies which demonstrate the typical cold pool structure and evolution and a summary analysis of IOP cases to support the generality of the behaviour shown. The ground-based station data are treated in groups corresponding to transects 1 to 6 identified in Figure 1.

4.1. Valley-bottom temperatures

Figure 2(a) depicts temperatures at different times during an IOP on 4–5 March 2010 in transect 5 along the Clun valley, during which clear, low wind conditions prevailed with little change overnight. Note that, where an AWS has been collocated with a HOBO or mast station in a transect, the HOBO or mast temperature only is plotted; this is for the sake of consistency with the majority of other instruments in the transects. At the start of the night, the valley atmosphere is well mixed in the vertical and temperature varies inversely with height. Subsequently, temperatures rapidly decrease, with the valley-bottom stations becoming colder than the valley head station (HOBO 19), reflecting the formation of a near-surface temperature inversion. Temperatures drop fairly evenly along the valley bottom, but with some variation between stations, and only in the coldest part of the night does the variation of temperature with height become monotonic, decreasing with distance down-valley. Figure 2(b), showing valley-bottom temperatures at the coldest time in the night for a selection of strong cold pooling nights, indicates that a degree of along-valley temperature variation is typical, with generally a down-valley decrease in temperature, particularly at HOBO 6 at the end of the transect, which is consistently the coldest site. Temperatures in transect 6 along the Burfield valley are also added for 4–5 March 2010. In transect 6, the decrease of temperatures with distance down-valley is more linear than in transect 5. However, in the initial hours of the night, the stations in the Burfield valley bottom cool at a similar rate to each other (not shown), similar to Figure 2(a).

Figure 3 contains equivalent comparisons for cross-valley transects in the Clun Valley. Figure 3(a) shows overnight variation along transect 3 during 4–5 March 2010. The growth of the temperature inversion within the valley during the night is clear, with the temperature decreasing much more rapidly at the valley bottom than at the valley sides. Figure 3(b) compares transect 3 for the same times as in Figure 2(b). Noticeable here are differences between nights in the variation of temperature with height between stations. On some nights the temperature decreases monotonically with depth into the valley, indicating that the inversion is deep enough to envelop the valley side stations. Interestingly, the cold pool on 7–8 January 2010, which is significantly more intense than others observed during the campaign, is comparatively shallow, with the inversion not reaching the valley side stations. This is probably an exceptional case, thanks to the presence of lying snow on that night, affecting surface energy fluxes. Transects 1–3 are compared in Figure 3(c) and 3(d) for two consecutive nights of 11–12 and 12–13 September 2009. These nights follow an IOP which marked the start of a period of five consecutive nights

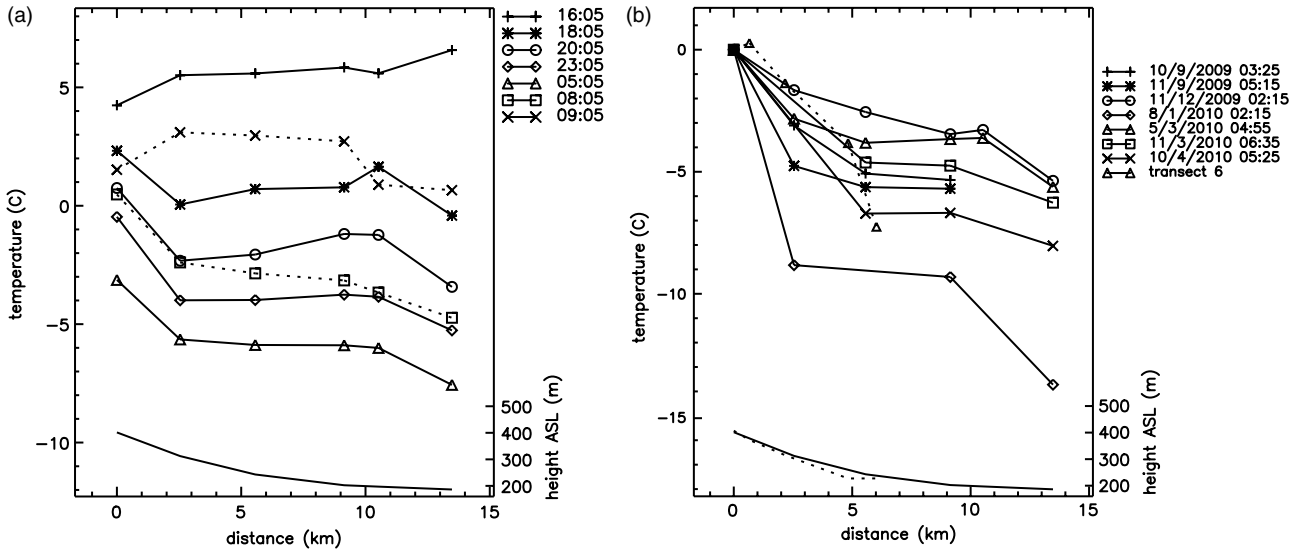

Figure 2. Behaviour of station temperatures in along-valley transects: (a) hourly plots of temperatures overnight along transect 5 in the Clun valley (Figure 1) during 4–5 March 2010, (b) comparison of temperatures along transect 5 for a selection of nights when strong cold pools occurred, at the time of the lowest temperature detected within the transect during each night. Temperatures in (b) are plotted relative to the temperature at the site at the head of the valley. Equivalent data for transect 6 in the Burfield valley for 4–5 March 2010 are labelled 'transect 6'. Heights of stations above sea level are indicated by lines at the bottom of each panel (dotted for transect 6 in (b)).

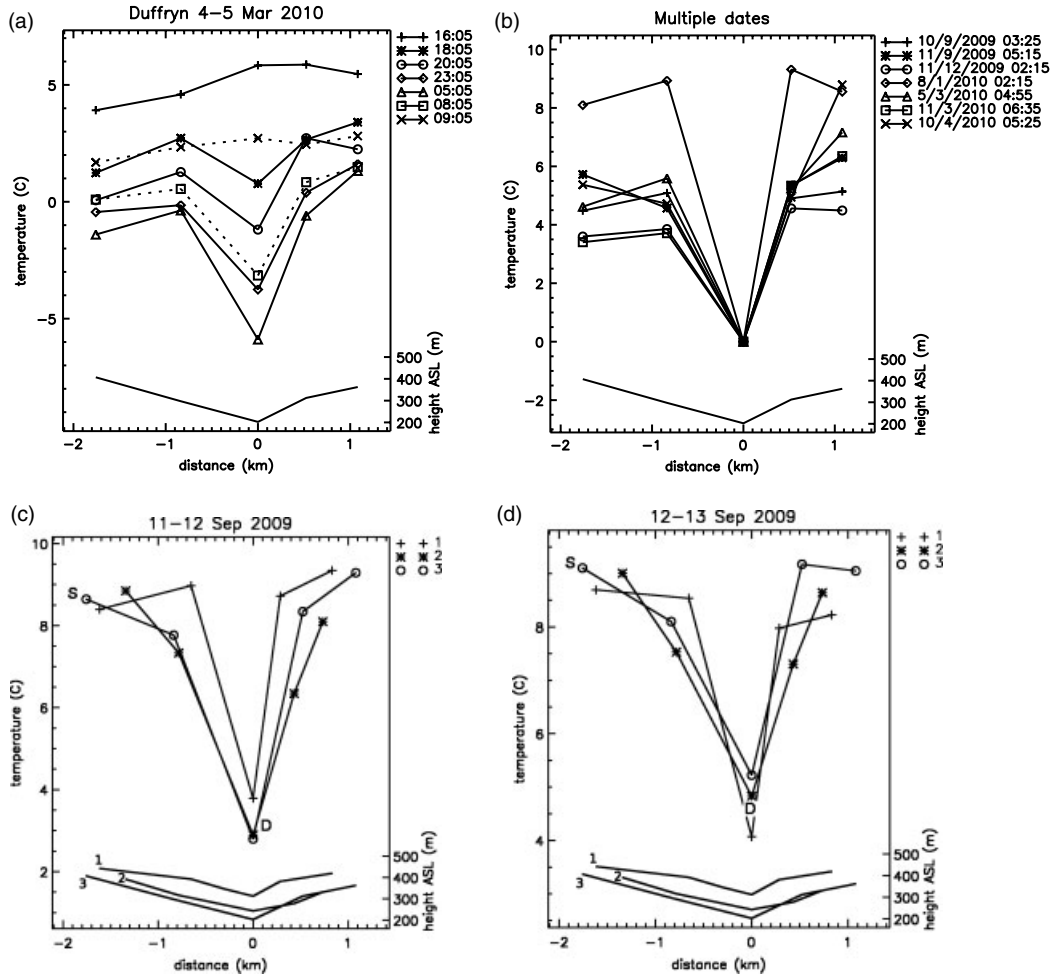

Figure 3. As Figure 2, but showing (a), (b) transect 3 across the Clun valley, and (c), (d) transects 1, 2 and 3 on 11–12 and 12–13 September 2009, respectively. Temperatures are plotted relative to the valley-bottom HOBO in (b). Duffryn and Springhill radiosonde release sites are marked 'D' and 'S' in (c) and (d).

of strong cold pools, during which synoptic conditions from one night to the next were very similar. Given the similarity in external conditions, the two cases give a measure of the natural variability of along-valley and cross-valley cold pool structure.

Figures 2 and 3 indicate that the cold pool structure near the surface is somewhat similar for different nights. In particular, the cold pool intensity is characterised by particularly strong falls in temperature at a string of stations along the valley bottom. The comparison between the Burfield and Clun valley bottoms in Figure 2(b) indicates some difference in character between the two valleys, with a more rapid rate of temperature decrease with distance down-valley in the Burfield valley. Examining first the Clun valley, the similarity in temperature between some stations (e.g. HOBO 13, the Duffryn mast, HOBO 2 and AWS 9) may reflect topographic similarity between their locations. HOBO 6, on the other hand, is significantly colder during cold pool episodes and this may be a consequence of confluence of large tributaries and broadening of the valley at this point, increasing the effective upstream 'catchment area' of cold air (for instance if drainage makes a contribution to the local cooling). Meanwhile, in Burfield valley, the local topography at each station is quite different. A narrow 'neck' separates the bowl-shaped valley head area containing the Burfield mast from the valley's lower portion, and again the coldest station in the transect during strong cold pools, HOBO 7, lies in a significant area of valley broadening and confluence. In addition, the Burfield mast is situated away from the river bed on a small local plateau within the valley, which may increase its contrast with the lower-lying stations. Also, sheltering effects isolating the coldest areas from turbulent mixing can be very localised and may result in local temperature biases in stable conditions. Such differences suggest that, in order to determine cold pool intensity representatively in each of the two valleys, a combination of stations along each valley bottom should be used. A further justification for this approach is the occurrence of local variations which were often observed when conditions were more variable during the night than in the cases shown.

4.2. *Comparison of surface stations with valley soundings*

An examination of cold pool structure is not complete without considering temperatures away from the surface within the greater part of the valley volume. Radiosondes released from Duffryn and Burfield, combined with the ground-based site data on the valley sides, offer an insight into how temperatures vary within vertical cross-sections through the valley. Whiteman *et al.* (2004a) presented cases where in general sensors on the sidewalls of the Gruenloch basin, Austria, compared closely with tethersonde vertical profiles of temperature above the basin floor overnight, but

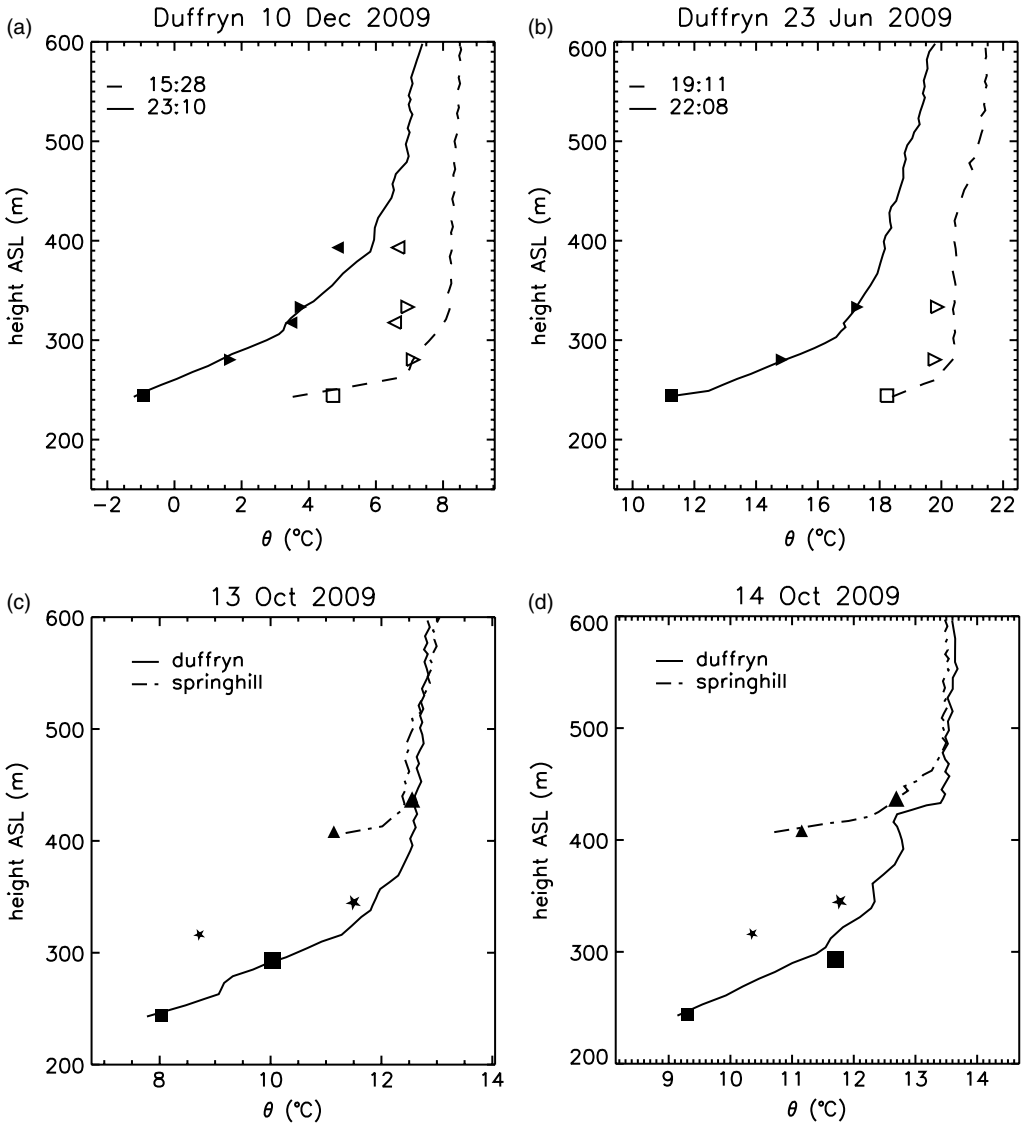

Figure 4. Comparisons of temperature measurements as a function of height above sea level from ground-based sites and contemporaneous radiosonde releases (a), (b) from the same location at different times, and (c), (d) from different locations at the same time. In (a) and (b), ground-based measurements are 10 min average screen temperatures from sites in transect 2 (Figure 1), with mast temperatures plotted as squares, HOBO temperatures as left- pointing triangles (south slope) and right-pointing triangles (north slope). In (c) and (d), these are 10 min averages from the Duffryn (squares), Springhill (triangles) and Burfield (stars) masts at screen level (small symbols) and mast tops (large symbols), and radiosonde releases are from Duffryn and Springhill at (c) 1905 and 1911 UTC on 13 October 2009, respectively, and (d) 2102 and 2101 UTC on 14 October 2009.

where the highest sidewall stations tended to be colder on average by up to several degrees than the tethersonde profile. Hoch *et al.* (2011) show significant air–surface temperature differences occurring during METCRAX, larger ($\sim 6\,^{\circ}$C) towards the start of the night than later when the cold pool is well established ($\sim 2\,^{\circ}$C), and show how these can have a strong effect on the radiative flux divergences cooling the air within the cold pool. Meanwhile, the difference between near-surface air temperatures in complex terrain, and nearby 'free air' temperatures at the same elevation away from the surface, have been highlighted as a potential source of error in understanding climate change impacts (Pepin *et al.*, 1999; Pepin and Seidel, 2005; Marshall *et al.*, 2007; Daly *et al.*, 2009). Presumably, on clear, calm nights, since the surface is cooling radiatively, in turn cooling air adjacent to it, temperatures near the valley walls will generally be lower than those at the same height above sea level over the valley centre. As well as defining the thermal structure of cross-sections through the valley volume, the horizontal temperature gradients implied by this will be a driver for thermal flows and redistribution of cold air within the valley, impacting how the cold pool thermal structure subsequently evolves.

Figures 4(a) and (b) compare potential temperature profiles from sondes, and stations in transect 2 across the valley through Duffryn, for sonde releases during the nights of two IOPs: 10 December 2009 (fog formed later this night, but the analysis focuses on the period preceding this) and 23 June 2009, respectively, during which behaviour was typical of strong cold pools in general. Potential temperatures have here been calculated using the sonde pressure profiles. The data shown represent sondes which were released at times close to sunset and later, when the cold pool was fully established in each case. At 1528 UTC on 10 December 2009 (Figure 4(a)), there is a sharp, shallow linear temperature inversion directly above Duffryn, and a weaker inverted layer above this. One valley-side station lies within the lower layer, with a temperature close to that measured by the sonde at

the same height. The other stations at the valley sides are colder than the profile above Duffryn. The difference between the valley-side stations and sonde profile is also qualitatively similar for 23 June 2009 (Figure 4(b)). Later on, the inversion above Duffryn becomes much deeper (solid lines and symbols in Figures 4(a) and (b)) and the valley-side site potential temperatures have largely converged with the sonde temperature profile.

In order to interpret this behaviour in terms of cross-sectional temperature structure within the developing and mature cold pool, an assumption must be made concerning the vertical variation of temperature above the different measurement sites within the cross-section. Figures 4(c) and (d) compare data from sonde measurements taken on two consecutive nights, released in pairs roughly simultaneously from Duffryn and Springhill. Data from the three masts at screen level and at 50 m or 30 m (depending on the mast) are also included. These exemplify how, near the surface, the inversion layers above both Duffryn and Springhill tend to be similar, despite having very different exposure characteristics. At all three mast sites, the profiles from the masts are similar. It seems fair to assume that inversions above the valley-side sites are not dissimilar, given the similar offset of their screen temperatures from the sonde profile. Given this, the similar potential temperatures at the valley-side sites around sunset (dashed lines and hollow symbols in Figures 4(a) and (b)) suggest that isentropes across the valley are initially roughly terrain-parallel, with similar cooling occurring at all points. The later convergence of the valley-side site temperatures with those measured by the radiosondes (solid lines and symbols in Figures 4(a) and (b)) implies cross-valley isentropes are horizontal within the mature cold pool. The two dates shown are good examples of this convergence but, generally speaking, when the valley-bottom inversion top rises sufficiently above a given station in this transect, that station's temperatures will cluster around the radiosonde temperature at the same level.

Figures 5(a) and (b) show comparisons between ground-based site potential temperatures in transect 5 along the Clun valley and sondes released at Duffryn, and transect 6 along the Burfield valley and sondes released from Burfield, respectively, at the same times as those in Figure 4(a). Figure 5(a) shows that, unlike for Figures 4(a) and (b) representing a cross-valley section, even when the cold pool is mature, the temperatures along the valley floor are significantly lower than those from the sonde profile above Duffryn at the same height – in other words colder than the valley sides at the same height. This is consistent with a deeper inversion above the valley bottom compared to the valley sides at a given terrain height. It also indicates that isentropes in the mature cold pool are not horizontal at any time but retain a down-valley slope (i.e. are lower further down the valley) throughout the night. While such behaviour seems less clear for the Burfield valley (Figure 5(b)), this may be related to the shorter extent of the valley as discussed later in this section.

In order to generalise these findings regarding cold pool morphology, the reduction of site temperatures relative to the sonde temperature at the same height for transects 3, 5 and 6 were analysed for a set of eight IOP cases during which relatively constant conditions of cloud and background wind occurred through the night; the cases represent a range of cold pool strengths, though most involved strong cold pools. One of the cases is the night of 10–11 December 2009. Again, since fog formed halfway through this night, the latter part of that night has been excluded. The analysis involved comparison of values of $\Delta\theta_{\mathrm{site}} = \theta_{\mathrm{site}} - \theta_{\mathrm{sonde}}$ with values of $\Delta\theta_{\mathrm{sonde}} = \theta_{\mathrm{sonde}} - \theta_{500\,\mathrm{m}}$, where θ_{site} is the screen potential temperature at the surface site, θ_{sonde} the potential temperature from the contemporaneous radiosonde ascent at the same height, and $\theta_{500\,\mathrm{m}}$ the temperature of the same sonde at 500 m above sea level (asl). $\Delta\theta_{\mathrm{sonde}}$ reflects the degree of cooling of the valley atmosphere at a given level, increasing in magnitude as the valley-bottom inversion reaches and exceeds that level. (The height of 500 m was chosen as being close to, but significantly above, nearby hilltops and thus representing the background airmass.) These comparisons for the eight cases are shown in Figures 6(a)–(f) for transects 3, 5 and 6. Sondes were released from Burfield only during some of the IOPs, so there are fewer data in these plots; also most sondes from all release sites were released at night.

During the day, horizontal temperature gradients are usually relatively small, and almost exclusively positive

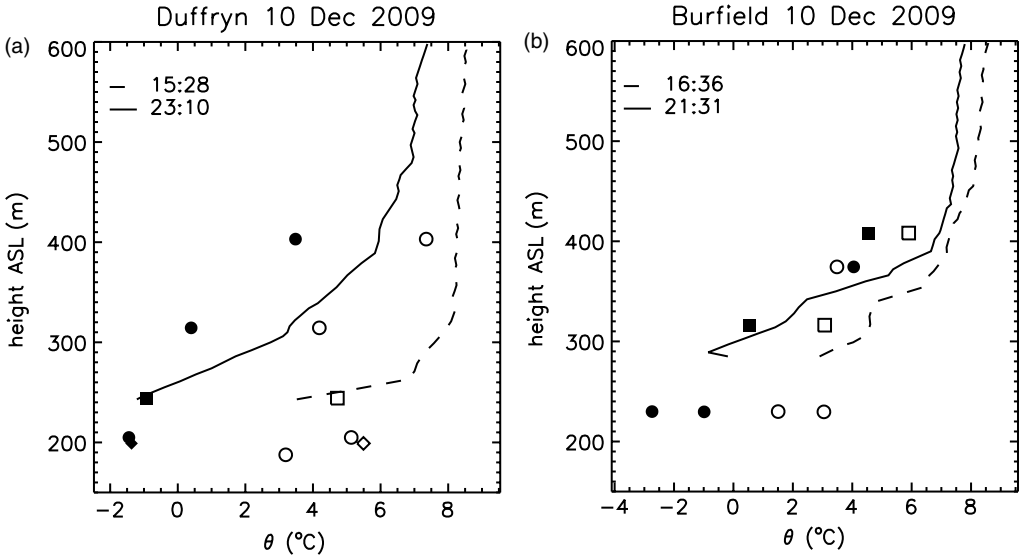

Figure 5. As Figures 4(a) and (b), but for sites in (a) transect 5 and (b) transect 6, and all HOBOs are plotted as circles.

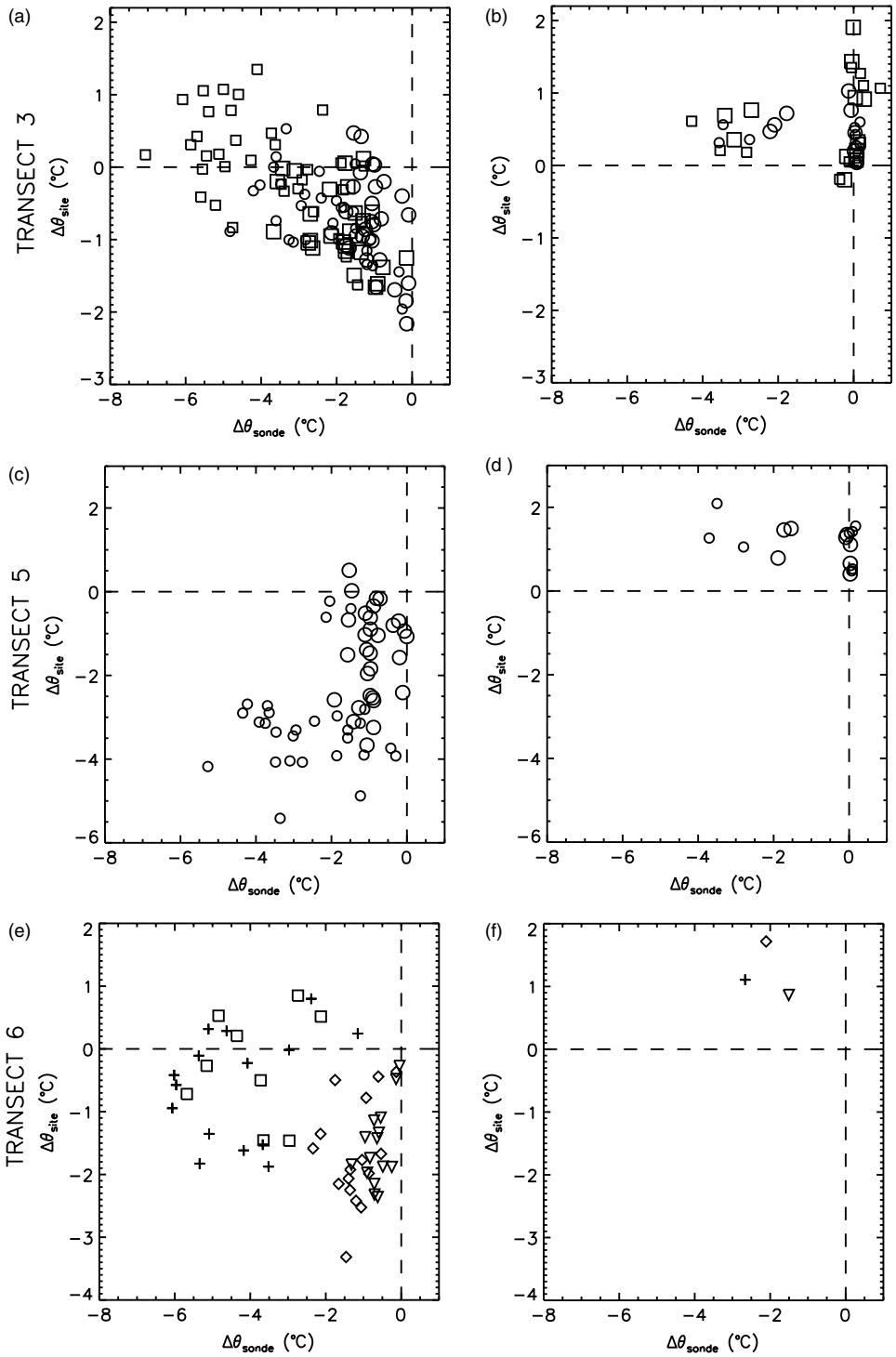

Figure 6. $\Delta\theta_{site}$ plotted as a function of $\Delta\theta_{sonde}$ (see text for definitions) for a selection of eight IOP dates. The three rows represent transects 3, 5 and 6 from top to bottom. The left and right columns represent night-time and daytime, respectively. In (a) and (b), circles represent the pair of stations on the south valley side, squares the pair on the north valley side, with the larger symbols the higher of each pair. In (c) and (d), larger circles again represent the higher of the two stations involved. In (e) and (f), triangle, rhombus, cross and square symbols represent the four different stations involved, in down-valley order.

values of $\Delta\theta_{site}$ for all three transects reflect daytime instability. $\Delta\theta_{sonde}$ values generally cluster close to zero as the valley atmosphere is well-mixed, except for data corresponding to several sondes during 10–11 December 2009, when a layer of fog persisted in the valleys, maintaining lower temperatures.

During the night, the behaviour of the three transects is distinctly different. For transect 3, across the Clun valley (Figure 6(a)), when the valley-bottom inversion is shallow and $\Delta\theta_{sonde}$ is close to zero, $\Delta\theta_{site}$ values are negative for all sites (all symbol types), reflecting behaviour closer to sunset (earlier times in Figures 4(a) and (b)). As the valley-bottom inversion deepens, and hence $\Delta\theta_{sonde}$ at a given site decreases (becoming more negative), $\Delta\theta_{site}$ values increase, so that eventually the preference for negative values disappears when the valley-bottom inversion top lies sufficiently high above the site. This indicates mature cold pools, to which the later times in Figures 4(a) and (b) correspond. Some scatter

in $\Delta\theta_{site}$ remains for all values of $\Delta\theta_{sonde}$; temperature fluctuations due to small vertical air motions are likely to be significant in size in such stable conditions. For transect 5 lengthwise along the valley (Figure 6(c)), no particular trend occurs for either site (note only two sites lie above the sonde release site in this transect) and $\Delta\theta_{site}$ values remain almost exclusively negative, as occurs in the example in Figure 5(a). An apparent trend of positive correlation in the data in Figure 6(c) is due to significantly larger values of $\Delta\theta_{site}$ at HOBO 13 than HOBO 19. HOBO 13 was sited some way along the valley bottom, whereas HOBO 19 was located within a relatively exposed 'saddle' at the valley head (Figure 1). Hence significantly greater cooling at the former location is consistent with terrain sheltering effects of the kind discussed by Vosper and Brown (2008). It is also possible that local terrain effects on a smaller scale at HOBO 13 make some contribution.

Figure 6(e) shows $\Delta\theta_{site}$ versus $\Delta\theta_{sonde}$ for transect 6 along the Burfield valley. Here, similarly to Figure 6(c) for transect 5, $\Delta\theta_{site}$ values are predominantly negative and it is difficult to discern any particular trend for individual sites. Though the overall trend in the plot is perhaps akin to that in Figure 6(a) for the cross-valley transect, here a tendency toward negative values of $\Delta\theta_{site}$ persists for all $\Delta\theta_{sonde}$. There are no stations in transect 6 for which $\Delta\theta_{site}$ values are noticeably much larger than for other stations, as occurs for HOBO 13 in transect 5. However, of the four stations in transect 6 analysed, two are in exposed locations near or above the valley head. For the other stations, local terrain effects (the Burfield mast and AWS 1 are located on a small local plateau) may play some part.

The magnitudes of $\Delta\theta_{site}$ are significantly larger in Figure 6(c) particularly, but also in Figure 6(e), than in Figure 6(a) (note the different axis scales). It could be argued that the significantly longer horizontal distances involved in transect 5 (roughly a factor of 4 difference in scale for the part used to plot Figure 6(b)) may be partly responsible for this since larger temperature differences will be easier to sustain over longer distances. For instance, scaling $\Delta\theta_{site}$ by the distance of the site from the ascent at the same level would reverse the above comparison of magnitudes. However, these details do not change the main observation that an along-valley horizontal potential temperature gradient persists throughout the cold pool life cycle, while cross-valley gradients disappear in the mature cold pool.

5. Case-study analysis of the influence of external conditions

In order to demonstrate the variation of temperatures within the COLPEX array during different external conditions, timeseries of the Duffryn and Burfield screen potential temperatures overnight for three case studies are included in Figures 7–9. The figures also contain timeseries of background conditions, including NH/U based on the hourly UK4 data (section 3). H in this study was determined using a 100 m resolution digital elevation model, by subtracting the height above sea level of the site from the mean height above sea level of the local terrain within a 2 km radius. For the mast sites, it is convenient to define potential temperature as $\theta = T - \Gamma\Delta h$, where $\Gamma = -0.0098\,\mathrm{K\,m^{-1}}$ is the dry adiabatic lapse rate and Δh is the difference in height between Duffryn and the site in question. In a test using a radiosonde ascent, the error in $\theta - T$ resulting from this approximation never exceeded 0.1 °C below 500 m above ground. The Springhill 30 m potential temperature has been plotted instead of the screen value since, of all available measurements, this is likely to be the least sensitive to nocturnal near-surface cooling, so that strictly local, diurnal variations occurring at the two valley mast sites are highlighted better. Figure 7 represents 3–4 August 2009, a windy, overcast night where the boundary layer is well mixed, and the neutral stratification is reflected in the close manner in which the potential temperatures at the three sensors follow each other, to within ∼ 0.5 °C.

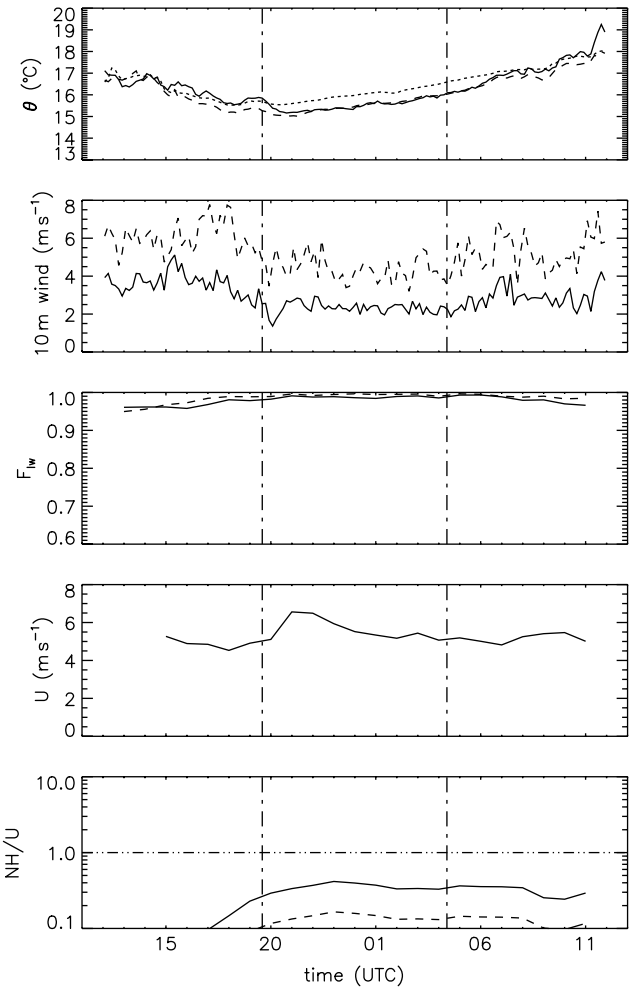

Figure 7. Timeseries of mast and vertical profile data for the cloudy, windy night of 3–4 August 2009. The quantities plotted are 10 min averages of observed potential temperatures at screen level, 10 m wind speed and 2 m F_{lw} (see text), and UK4 hourly wind, U, and NH/U. Solid lines denote data at Duffryn, dashed lines data at Burfield and dotted lines data at Springhill. Vertical dash-dot lines indicate sunset and sunrise times. NH/U values for the Clun and Burfield valleys differ only through the value of H, and hence the two traces in the bottom panel appear parallel.

Figures 8 and 9 represent nights when strong cold pools occurred, with the valley temperatures diverging from the Springhill trace to much lower values. A nominal level where NH/U would be equal to 1 has been added to the appropriate panels. Later analysis (section 6) suggests a critical value of around 1 is more appropriate for the observations than a value in the range 0.35–0.64 found by Vosper and Brown (2008). This may be related to the complex 3D structure of the valley terrain, which is effectively more exposed than an infinite 2D valley (lower

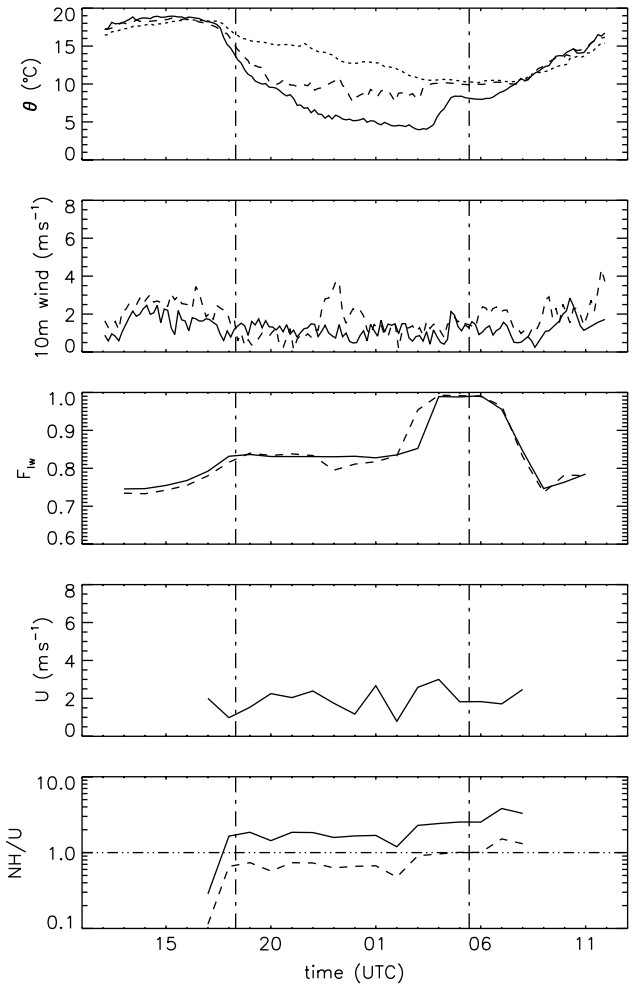

Figure 8. As Figure 7, but for 12–13 September 2009.

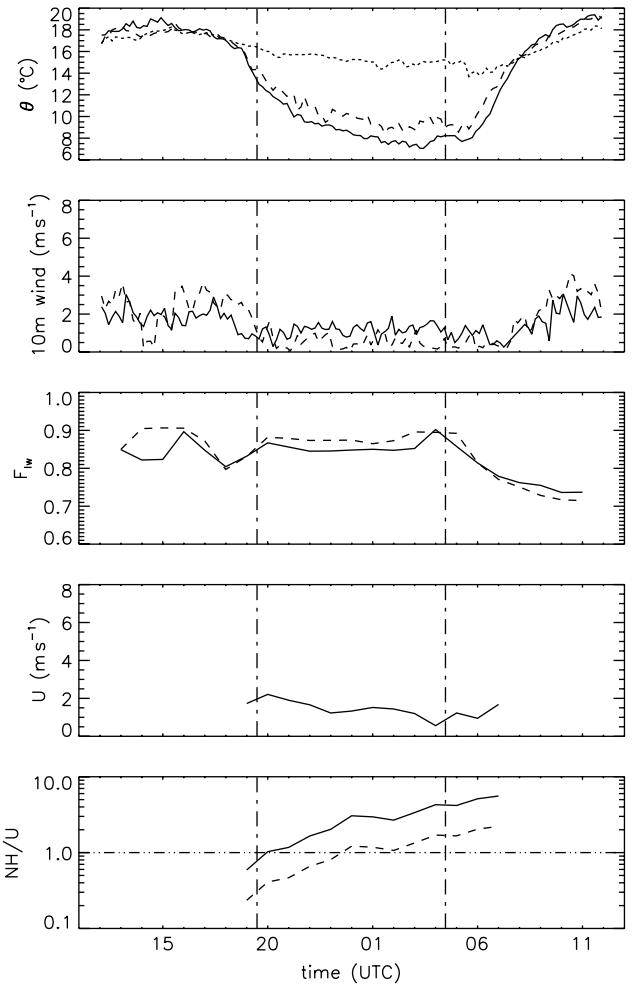

Figure 9. As Figure 7, but for 8–9 August 2009.

effective value of H), though Bell and Thompson (1980) also observed a higher value of critical NH/U. Low values of F_{lw} were recorded at the mast sites indicating strong radiative cooling and the UK4 average winds were below 3 m s^{-1} for both of these cases. However, on 12–13 September 2009 (Figure 8), while the value of NH/U at Duffryn quickly exceeds 1, suggesting probable decoupling there, NH/U does not increase above 1 at Burfield, suggesting the latter may not become completely decoupled. This appears to be borne out by the fact that the Burfield temperature does not drop as fast as that at Duffryn, eventually levelling out before cloud moves in later in the night and the cold pool disperses. At 2200, the hour by which the temperatures at Duffryn and Burfield have conclusively begun to diverge, the winds at Burfield increase briefly, probably representing momentum transferred down from aloft, or an intrusion of flow into the valley, effects from which Duffryn appears to remain sheltered. While the conditions are ostensibly similar on 8–9 August 2009 (Figure 9; indeed radiative cooling is slightly weaker), NH/U continues to increase during the night well beyond $NH/U = 1$ for both valleys, suggesting both valleys would have become decoupled. Again this appears to be reflected in the variation of temperatures. Although its temperature does not fall quite as fast at the start of the night, the temperature at Burfield closely follows that at Duffryn for the remainder of the night, unlike in the previous case. The 10 m winds remain low at both sites, which are apparently sheltered from the external flow. The slightly slower initial cooling at Burfield may reflect the later time at which it becomes decoupled. The site is also on a slightly raised area next to the river bed in the valley and is thought to be warmer than the valley bottom, which may also be responsible for the slight difference between the two valley mast sites. A systematic analysis of cold pool behaviour as a function of the variables in Figures 7–9 for the dataset as a whole follows in section 6.

The manner in which NH/U increases during the night of 8–9 August 2009 is typical of such cases in the dataset, and reflects the increasingly stable conditions occurring in the UK4 forecast, a realistic response to the clear, calm night-time conditions. Similarly, the results obtained using nocturnal averages to calculate NH/U in the idealised simulations of Vosper and Brown (2008) do not represent a static nocturnal state, but an evolving one which is successfully summarised using nocturnal averages. While instantaneous values of NH/U have a precise influence on flow dynamics at a given time, nightly averages represent a mixture of states, occurring during progressive stages of the night, even under the controlled conditions of idealised simulation. In real valleys, overnight averages mask even more complexity: Figure 8 demonstrates how cold pools may quickly be disturbed or removed by changes in external conditions; note the effect of the onset of overcast conditions in the early hours. Thanks to the moist midlatitude situation of the experiment, changing conditions due to the passage of weather systems, variability in cloud cover and wind

and formation of fog, were common. Different observed cold pool evolution scenarios for the Gruenloch sinkhole resulting from changes in conditions outside the valley were summarised and explained by Dorninger *et al.* (2011), and a similar degree of variety was evident during COLPEX. The implications of this for summarising overnight valley and external conditions in single quantities are discussed in the next section. However, a detailed examination of the temporal structure of the cold pools observed is beyond the scope of this article.

6. Quantitative relationship of cold pool intensity to external conditions

This section focusses on demonstrating how the intensity of a cold pool on a given night is influenced by external conditions. Methods are first introduced of summarising the overnight behaviour of the cold pool and external background by average parameters representing the whole night.

6.1. Cold pool intensity

The method of Vosper and Brown (2008) using the largest overnight relative temperature reduction, $\Delta\theta_{\min}$ in the valley to determine cold pool intensity is unlikely to be the best measure for real valleys for a number of reasons. Instrumentation is not sufficiently dense to be confident of measuring the lowest valley temperature (in any case, in a real valley, the lowest temperature may be the result of a terrain detail, rather than representative of the valley as a whole). Also, unlike the case with idealised simulations, there is a high likelihood of variation in conditions overnight, so that the valley minimum temperature does not meaningfully reflect the overnight cold pool evolution (both temporally and spatially). For instance, a single very brief cold pool due to a break in cloud and/or a calm period, and a night where the cold pool strength oscillates in response to variations in cloud cover and wind throughout the night could easily have the same $\Delta\theta_{\min}$. Meanwhile, quantities representing overnight external conditions would be different for each of these two cases, so that there is not a unique relationship between the cold pool intensity and the external quantities. Possible spatial variation in conditions when cloud is partial or wind variable suggests that a number of stations should be used to represent the degree of cooling in the valley. Furthermore, the discussion in section 4 indicates how systematic spatial variability is also present in the valley-bottom temperatures by virtue of their location. In practice, therefore, the Springhill 10 min average potential temperature minus the 10 min average potential temperature over the valley-bottom sites has been used as a measure of cold pool intensity at a given time. This was then averaged overnight to represent the overnight cold pool intensity, $\Delta\theta$. The sign convention used is such that cold pools result in a positive value of $\Delta\theta$. It is noticeable in Figures 8 and 9 that valley potential temperatures tend to first decrease (indicating a cold pool beginning to form) before sunset and do not recover until a time after sunrise. For this reason, when calculating averages, the night is assumed to start at the typical time of evening transition for the time of year (calculated according to a method used by Lapworth and Claxton, 2010), roughly two to three hours before sunset, and to end the same amount of time after sunrise. For Clun valley, the valley-bottom sites used comprise HOBOs 2, 6 and 13 and the Duffryn mast (due to some gaps in the dataset, AWS 9 has not been used, in order to maximise the number of nights for which averages can be performed over the same set of stations). For Burfield, the Burfield mast, AWS 1 and HOBOs 7 and 22 were used (when data from both the Burfield mast and AWS 1, which were collocated, were available, each was weighted by a half).

Other options for representing the cold pool using the initial period of the night when cooling is strongest (and arguably sheltering is most relevant), or attempting to guess the most representative site (e.g. the furthest down-valley) instead of averaging over all valley-bottom sites, were found to produce substantially noisier relationships which most likely suffer from the spatial and temporal sampling issues discussed above.

The calculation described above in effect integrates the temperature reduction within the cold pool overnight and in this respect resembles the method used by Yao and Zhong (2009) to quantify cold pools in Arizona's Meteor Crater.

6.2. Parameters of the external flow

Nocturnal averages of the N and U values based on UK4 data as described in section 3 were calculated, representing a direct analogy to $\widetilde{N}$ and $\widetilde{U}$, the overnight averages used by Vosper and Brown (2008) to determine non-dimensional valley depth, $\widetilde{N}H/\widetilde{U}$. In order to determine a non-dimensional valley depth for the observations, the effective valley depth, H, determined as described in section 5, was used. This measure of valley depth reflects the shape of the surrounding terrain and how well it may provide shelter (very wide valleys with many tributary entries around a site providing little or no shelter, narrow closed basins providing the most shelter). Since the valley-bottom sites are to be treated collectively, the final value of H is simply the average of the individual values for the sites named in subsection 6.1 in each valley. From here on NH/U refers to the parameter created using these averages of N, H and U.

A more sophisticated method such as determining 'up-valley catchment', in order to reflect the possible tendency for temperatures to decrease down-valley, might prove useful in describing spatial variations in the cold pool structure, but is unlikely to impact greatly on the average representative H and so has not been pursued here.

In order to represent radiative conditions overnight, the mean of nocturnal screen F_{lw} values at Duffryn was used. From here on F_{lw} refers to the nocturnal mean quantity.

6.3. Relationship of cold pool intensity to external flow parameters

Vosper and Brown (2008) found that, for a given valley, U and F_{lw} alone determine the cold pool strength (their Figure 11). The equivalent quantities are plotted for the COLPEX observations in the Clun valley in Figure 10(a). Here also U and F_{lw} explain the great majority of variation in $\Delta\theta$. The remaining variability is likely related to factors such as variability in wind and radiative conditions during the night. Different patterns of variability will affect overnight averages in different ways, since the variation of $\Delta\theta$ does not have a linear dependence on the instantaneous values of U and F_{lw}.

Plots of $\Delta\theta$ for the Clun valley as a function of non-dimensional valley depth are shown in Figures 10(b) and (c),

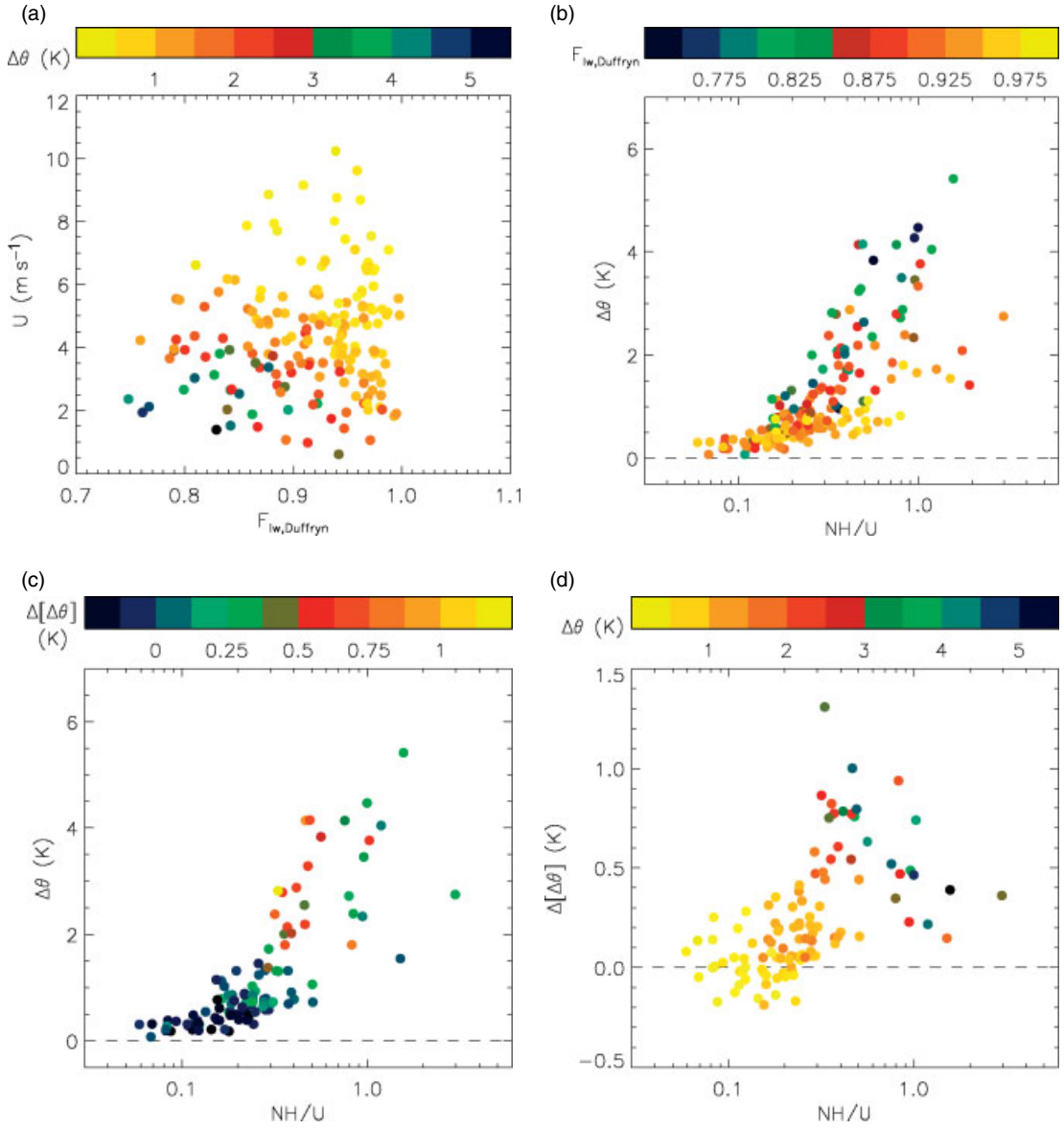

Figure 10. (a) Variation of cold pool intensity $\Delta\theta$ (see text, plotted as symbol colour) in the Clun valley, as a function of overnight average F_{lw} and U at Duffryn. (b) Variation of $\Delta\theta$ as a function of non-dimensional valley depth for the Clun valley, with colour representing the value of F_{lw} at Duffryn. (c) is as (b), but with colours representing the difference $\Delta[\Delta\theta]$ (see text) between the Clun and Burfield valleys. (d) Variation of $\Delta[\Delta\theta]$ as a function of non-dimensional valley depth, with colour representing $\Delta\theta$ for the Clun valley (i.e. simply swapping the vertical axis and colour axis variables in (c)). Note there are fewer points in (c) than in (b) due to the constraint that sufficient good data must be available for Springhill and all valley-bottom stations in both valleys for (c).

highlighting different values of F_{lw} and $\Delta[\Delta\theta]$, respectively. $\Delta[\Delta\theta]$ represents the difference in $\Delta\theta$ between the Clun and Burfield valleys. This is determined by replacing Springhill potential temperatures with the average values from the Burfield valley in the calculation of $\Delta\theta$. The $\Delta[\Delta\theta]$ values themselves are plotted in Figure 10(d). Only nights where data from Springhill, from all four sites for Clun valley and all three distinct sites for Burfield valley were available for 80% of the night are permitted in the analysis for Figure 10(c). Equivalent criteria were applied for Clun valley and Springhill for Figures 10(a) and (b), and Clun valley and Burfield valley for Figure 10(d).

The expectation based on Vosper and Brown (2008) is that, as NH/U increases, the strength of the cold pool also increases until, beyond the critical NH/U, it plateaus at some peak value which depends on U and F_{lw}. Figure 10(b) is consistent with this, cold pool strength increasing with NH/U, with the suggestion (looking at points with similar F_{lw}, indicated by colour) that the critical NH/U is perhaps somewhere between 0.5 and 1.0. The colours show that smaller F_{lw} generally leads to stronger cold pools, again consistent with expectations. Since for obvious reasons the ratio NH/U is very strongly linked to the values of U and F_{lw} for a constant H (it was found that 78% of the variance in $log(N/U)$ was explained by linear regression in U and F_{lw}), Figures 10(a) and (b) are broadly speaking expressing the same behaviour. However, the relationship in Figure 10(b) has the advantage of applying generally, for valleys of any depth.

In order to test the generality of this dependence on NH/U independently of U and F_{lw}, it is necessary to investigate the effect of varying H without changing external atmospheric conditions. This was the method used by Vosper and Brown (2008) to establish the importance of the non-dimensional valley depth in their study. The Clun and Burfield valleys are of different depths and thus afford the opportunity to

investigate the effect of changing NH/U by changing H for a given N/U. As NH/U increases, the expected difference in potential temperature between two such valleys for a given F_{lw} and U would increase to a peak at the point of strongest sensitivity to NH/U, somewhere between strongly coupled and completely decoupled behaviour. After this peak, as NH/U increases further, both valleys are at some point expected to become decoupled and contain cold pools of the same strength. The data points in Figure 10(c) have been coloured according to the average of the overnight potential temperature difference between the two valleys, $\Delta[\Delta\theta]$, and show that this indeed occurs. On the left of the plot, cold pools are weak and little difference occurs between the two valleys. In the central part of the NH/U range, between around 0.25 and 1.00 where cold pool strength for given ambient conditions is changing rapidly with increasing NH/U, the difference is relatively large (indicated by the red/orange/yellow dots), particularly for stronger cold pools. At larger NH/U values, the difference between the two valleys again decreases to small values, even for the strongest cold pools observed, indicating cold pools of similar strength in the two valleys. $\Delta[\Delta\theta]$ itself is plotted in Figure 10(d), and shows this more clearly. Larger values of $\Delta[\Delta\theta]$ occur in the centre of the NH/U range, with smaller values at low NH/U and again at the largest values of NH/U. The colours in Figure 10(d) represent $\Delta\theta$ in the Clun valley (y-axis values of Figure 10(b)), from which, for instance, it is clear that for the strongest cold pools (green and blue colours) $\Delta[\Delta\theta]$ decreases with increasing NH/U, suggesting approach towards the critical value of NH/U. Figures 10(c) and (d) suggest a critical NH/U in a region close to 1.

The above analysis qualitatively establishes the influence of NH/U on cold pool behaviour, and its generality for the two valleys. It is possible to establish this more quantitatively by demonstrating that a change in NH/U has an effect on cold pool strength which is of the same magnitude regardless of whether it is brought about by changing N and U, or by changing H. The largest values of the difference in cold pool strength, $\Delta[\Delta\theta]$, between the two valleys occur around $NH/U = 0.4$ (Figure 10(d)). By determining the gradient of $\Delta\theta$ versus NH/U for points with small F_{lw} in Figure 10(b) (blue and green points) in the range $0.2 < NH/U < 0.6$, an estimate of the peak $\Delta[\Delta\theta]$ of 1.27 K was obtained, based on the difference in NH/U between the two valleys. The peak observed difference in cold pool intensity between the valleys is $\Delta[\Delta\theta] = 1.31$ K, occurring at $NH/U = 0.31$ for a case with small F_{lw} (Figure 10(d)).

Clearly the parameters in Figure 10 do not fully account for all variability in the data; significant scatter occurs. The fact that this occurs even for cases without cold pool formation (e.g. Figure 10(d) at small NH/U) suggests that a large part of this is the effect of background variability in the quantities studied, as opposed to being due to any shortcomings of the conceptual model followed. Other sources of scatter include the effect of comparing averages overnight of quantities that are variable in time, but do not vary linearly with each other (for instance, an average overnight value of $NH/U = 0.5$ could mean half the night close to zero (nearly neutral) and the remainder at values close to 1 (decoupled), or could mean $NH/U = 0.5$ throughout, with different implications for average cold pool intensity in the two valleys). Also, even in the idealised simulations of Vosper and Brown (2008), not a single critical value, but rather a range of critical values of NH/U were found for different combinations of U and F_{lw}. It is further likely that fine-scale 3D processes such as drainage of cold air along the valley have some impact which is not accounted for. (Vosper *et al.*, 2013, find evidence of a significant drainage current down the Clun valley.) Remaining factors include the problem of obtaining representative valley average temperatures from a relatively small number of valley-bottom stations, the effect of external wind direction, UK4 forecast data quality, and topological differences between the Clun and Burfield valleys.

7. Conclusions

Characteristics of strong cold-air pools in a system of small UK valleys O(1km) have been studied using measurements in cross-sections across and along the Clun valley, and along the Burfield valley. For nights during which wind, stability and moisture change little, cold pools are found to have a fairly generic structure and development over time once nocturnal cooling begins. During the daytime, the valley atmosphere is essentially well-mixed, with all surface locations within the valley having similar screen potential temperatures. As radiative net cooling of the surface begins, screen potential temperatures remain similar at different valley sites as all locations cool at similar rates and isentropes appear to be roughly terrain-parallel. As the night progresses, the inversion at the valley bottom deepens and isentropes across-valley become horizontal in a growing layer at the valley bottom. Meanwhile, along the valley isentropes appear to retain a down-valley tilt. This is consistent with high-resolution simulations by Vosper *et al.* (2013), in which this tilt provided thermal forcing for a persistent down-valley current during the night.

Case-studies confirm the well-known importance of strong net upwelling long-wave radiation and light winds, but also demonstrate the importance of the non-dimensional mountain height, NH/U, of the approach flow concerning the strength of cold pooling. In an analysis of the data as a whole, it was found that cold pool strength increases with NH/U, but that a critical value of NH/U exists above which cold pool strength no longer increases, consistent with idealised simulations of Vosper and Brown (2008). For instance, for nights with sufficiently large NH/U, two valleys of significantly different depth, H, were found to contain cold pools of similar strength. As in the Vosper and Brown study, the use of a method of NH/U calculation that is not affected by interaction of the approaching flow with the valley or the cold pool formation process was vital in obtaining a meaningful relationship between the behaviour of temperature in the valley and the flow conditions external to it. A simplified version of the dependence on NH/U is currently used operationally to post-process MetUM forecast temperatures for high-resolution forecasting (Sheridan *et al.*, 2010; Smith *et al.*, 2010). This work helps validate the approach and paves the way to further improvements.

It would be useful to perform similar analyses for other valley systems with differences in any of the following: valley geometry, scale, land-use, location relative to other terrain, and climate. Atmospheric moisture, flow confinement, the formation of strong katabatic flows, the impact of larger-scale orographic flow processes, and surface exchange

characteristics would all be expected to affect the behaviour of cold pools.

Acknowledgements

The authors gratefully acknowledge the participation and effort of those involved in planning and carrying out the COLPEX field campaign, in particular Jeremy Price and others at the Met Office (Cardington Meteorological Research Unit), and teams from the Universities of Leeds, Salford and Surrey.

References

Adler B, Whiteman CD, Hoch SW, Lehner M, Kalthoff N. 2012. Warm-air intrusions in Arizona's Meteor crater. *J. Appl. Meteorol. Climatol.* **51**: 1010–1025.

Bell RC, Thompson RORY. 1980. Valley ventilation by cross winds. *J. Fluid Mech.* **96**: 757–767.

Bodine D, Klein PM, Arms SC, Shapiro A. 2009. Variability of surface air temperature over gently sloped terrain. *J. Appl. Meteorol. Climatol.* **48**: 1117–1141.

Clements CB, Whiteman CD, Horel JD. 2003. Cold-air-pool structure and evolution in a mountain basin: Peter sinks. *J. Appl. Meteorol.* **42**: 752–768.

Daly C, Conklin DR, Unsworth MH. 2009. Local atmospheric decoupling in complex topography alters climate change impacts. *Int. J. Climatol.* **30**: 1857–1864.

Davies T, Cullen MJP, Malcolm AJ, Mawson MH, Staniforth A, White AA, Wood N. 2005. A new dynamical core for the Met Office's global and regional modelling of the atmosphere. *Q. J. R. Meteorol. Soc.* **131**: 1759–1782.

Dorninger M, Whiteman CD, Bica B, Eisenbach S, Pospichal B, Steinacker R. 2011. Meteorological events affecting cold-air pools in a small basin. *J. Appl. Meteorol. Climatol*, **50**: 2223–2234.

Gustavsson T, Karlsson M, Bogren RA, Lindqvist S. 1998. Development of temperature patterns during clear nights. *J. Appl. Meteorol.* **57**: 559–571.

Haiden T, Whiteman CD, Hoch SW, Lehner M. 2011. A mass-flux model of nocturnal cold air intrusions into a closed basin. *J. Appl. Meteorol. Climatol.* **50**: 933–943.

Hoch ST, Whiteman CD, Mayer B. 2011. A systematic study of longwave radiative heating and cooling within valleys and basins using a three-dimensional radiative transfer model. *J. Appl. Meteorol. Climatol.* **50**: 2473–2489.

Iijima Y, Shinoda M. 2000. Seasonal changes in the cold-air pool formation in a subalpine hollow, Central Japan. *Int. J. Climatol.* **20**: 1471–1483.

Kiefer MT, Zhong S. 2011. An idealised modeling study of nocturnal cooling processes inside a small enclosed basin. *J. Geophys. Res.* **116**: D20127, DOI: 10.1029/2011JD016119.

Lapworth AJ, Claxton BM. 2010. The effect of terrain on the evening wind. *Q. J. R. Meteorol. Soc.* **136**: 1763–1772.

Lean HW, Clark PA, Dixon M, Roberts NM, Fitch A, Forbes R, Halliwell C. 2008. Characteristics of high-resolution versions of the Met Office Unified Model for forecasting convection over the United Kingdom. *Mon. Weather Rev.* **136**: 3408–3424.

Marshall SJ, Sharp MJ, Burgess DO, Anslow FA. 2007. Near-surface-temperature lapse rates on the Prince of Wales icefield, Ellesmere Island, Canada: implications for regional downscaling of temperature. *Int. J. Climatol.* **27**: 385–398.

Pepin NC, Seidel DJ. 2005. A global comparison of surface and free-air temperatures at high elevations. *J. Geophys. Res.* **110**: D03104, DOI: 10.1029/2004JD005047.

Pepin N, Benham D, Taylor K. 1999. Modeling lapse rates in the maritime uplands of northern England: implications for climate change. *Arctic Antarctic Alpine Res.* **31**: 151–164.

Price JD, Vosper S, Brown A, Ross A, Clark P, Davies F, Horlacher V, Claxton B, McGregor JR, Hoare JS, Jemmett-Smith B, Sheridan P. 2011. COLPEX: Field and numerical studies over a region of small hills. *Bull. Amer. Meteorol. Soc.* **92**: 1636–1650.

Reeves HD, Stensrud DJ. 2009. Synoptic-scale flow and valley cold pool evolution in the western united states. *Weather Forecasting* **24**: 1625–1643.

Savage CL, Zhong S, Yao W, Brown WJO, Horst TW, Whiteman CD. 2008. An observational and numerical study of a regional-scale downslope flow in northern Arizona. *J. Geophys. Res.* **113**: D14114, DOI: 10.1029/2007JD009623.

Sheridan PF, Smith SA, Brown AR, Vosper SB. 2010. A simple height-based correction for temperature downscaling in complex terrain. *Meteorol. Appl.* **17**: 329–339.

Smith SA, Brown AR, Vosper SB, Murkin PA, Veal AT. 2010. Observations and simulations of cold air pooling in valleys. *Boundary-Layer Meteorol.* **134**: 85–108.

Steinacker R, Whiteman CD, Dorninger M, Pospichal B, Eisenbach S, Holzer AM, Weihs P, Mursch-Radlgruber E, Baumann K. 2007. A sinkhole field experiment in the eastern Alps. *Bull. Amer. Meteorol. Soc.* **88**: 701–716.

Vosper SB, Brown AR. 2008. Numerical simulations of sheltering in valleys: the formation of night-time cold-air pools. *Boundary-Layer Meteorol.* **127**: 429–448.

Vosper SB, Hughes JK, Lock AP, Sheridan PF, Ross AN, Jemmett-Smith B, Brown AR. 2013. Cold pool formation in a narrow valley. *Q. J. R. Meteorol. Soc.* DOI: 10.1002/qj.2160 (in press).

Whiteman CD. 1990. Observations of thermally developed wind systems in complex terrain. *Meteorol. Monogr.* **23**: 5–42. Amer. Meteorol. Soc: Boston, MA.

Whiteman CD, Eisenbach S, Pospichal B, Steinacker R. 2004a. Comparison of vertical soundings and sidewall air temperature measurements in a small Alpine basin. *J. Appl. Meteorol.* **43**: 1635–1647.

Whiteman CD, Haiden T, Pospichal B, Eisenbach S, Steinacker R. 2004b. Minimum temperatures, diurnal temperature ranges, and temperature inversions in limestone sinkholes of different sizes and shapes. *J. Appl. Meteorol.* **43**: 1224–1236.

Whiteman CD, de Wekker SFJ, Haiden T. 2007. Effect of dewfall and frostfall on night-time cooling in a small, closed basin. *J. Appl. Meteorol. Climatol.* **46**: 3–13.

Whiteman CD, Muschinski A, Zhong S, Fritts D, Hoch SW, Hahnenberger M, Yao W, Hohreiter V, Behn M, Cheon Y, Clements CB, Horst TW, Brown WOJ, Oncley SP. 2008. METCRAX 2006: Meteorological experiments in Arizona's Meteor crater. *Bull. Amer. Meteorol. Soc.* **89**: 1665–1680.

Whiteman CD, Hoch SW, Lehner M, Haiden T. 2010. Nocturnal cold-air intrusions into a closed basin: Observational evidence and conceptual model. *J. Appl. Meteorol. Climatol.* **49**: 1894–1905.

Yao W, Zhong S. 2009. Nocturnal temperature inversions in a small, enclosed basin and their relationship to ambient atmospheric conditions. *Meteorol. Atmos. Phys.* **103**: 195–210.

Zängl G. 2004. A re-examination of the valley wind system in the Alpine Inn Valley with numerical simulations. *Meteorol. Atmos. Phys.* **87**: 241–256.

Zängl G. 2005. Large-scale flow interactions with the Alps and their impact on the low-level temperature field in the northern foreland. *Meteorol. Z.* **14**: 379–386.

Zängl G. 2009. The impact of weak synoptic forcing on the valley-wind circulation in the Alpine Inn Valley. *Meteorol. Atmos. Phys.* **105**: 37–53.